Overshielding event of 28-29 July 2000

J. Goldstein[1], R. W. Spiro[1], B. R. Sandel[2], R. A. Wolf[1], S.-Y. Su[3], P. H. Reiff[1]

Abstract.

On 29 July 2000, IMAGE EUV observed a shoulder-like bulge on the afternoon sector plasmapause. *Goldstein et al.* [2002] showed that plasmaspheric shoulders may be caused by a pre-dawn concentration of eastward overshielding electric (E) field triggered by a decrease in magnetospheric convection. A simulation by the Magnetospheric Specification Model (MSM) captures the formation of the shoulder, reproducing its approximate size and location. ROCSAT-1 ion drift meter data are consistent with the strength, time development and local-time variation of the MSM eastward penetration E-field (and associated radial flows) during the shoulder formation on 28 July.

1. Plasmaspheric Shoulder of 29 July 2000

The IMAGE extreme ultraviolet (EUV) imager routinely obtains global images of the plasmasphere by detecting 30.4-nm light resonantly scattered by He^+. Between 1:35–9:56 UT on 29 July 2000, IMAGE EUV observed a shoulder-like bulge on the afternoon sector plasmapause, but did not observe its creation. The left panel of Fig 1 is an EUV snapshot from 2:57 UT on 29 July. In the center of the image, the black circle gives the apparent size and position of the Earth, as seen by EUV from its vantage point above the north pole. The white arrow is the Sun-direction. The plasmasphere is the bright red-orange region surrounding the Earth; the plasmapause is the outer boundary where the brightness drops off. The shoulder (labeled 'S') was asymmetric in magnetic local time (MLT) with a sharp eastern edge $\geq 1\,R_E$ in radial extent that gradually tapered off on the western side. In the right panel of Fig 1, the plasmapause is extracted from the EUV image and mapped to the magnetic equatorial plane (Sun to the right). The mapped plasmapause is the series of filled circles encircling the Earth at radial distances ranging 2.5–4 R_E. At 2:57 UT, the eastern edge of the shoulder ('S') was at 15 MLT, and its azimuthal center at noon MLT. Successive EUV images during 1:35–9:56 UT on 29 July show the shoulder moving eastward, approximately corotating with the Earth.

[1] Department of Physics and Astronomy, Rice University, Houston, TX 77005 USA

[2] Lunar and Planetary Laboratory, University of Arizona, Tucson, AZ 85721 USA

[3] Institute of Space Science, National Central University, Taiwan, Republic of China (ROC)

Paper number .
0094-8276/03/$5.00

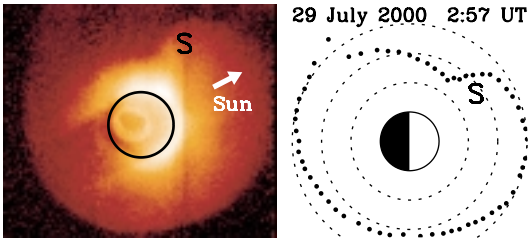

Figure 1. Left: EUV image, 2:57 UT, 29 July 2000, showing the plasmaspheric shoulder ('S'). Right: EUV plasmapause mapped to the magnetic equator.

2. Connection to Overshielding

Plasmaspheric shoulders in EUV images were identified and discussed by *Burch et al.* [2001a, b]. *Goldstein et al.* [2002] suggested that the 24 May 2000 shoulder was created by an overshielding condition that arose after sudden northward turnings of the interplanetary magnetic field. The earthward edge of the plasmasheet and finite-conducting ionosphere create an electric (E) field that shields the inner magnetosphere from convection, but this shielding is established on a time scale $\tau_S \leq 1$ hour [*Kelley et al.*, 1979; *Senior and Blanc*, 1984]. It has been assumed that convection variations slower than τ_S can be completely shielded, but sudden changes produce a residual 'penetration' E-field in the inner magnetosphere. A sudden southward IMF turning causes 'undershielding' (shielding is temporarily insufficient to balance the newly enhanced convection). A rapid northward IMF turning decreases convection, creating a temporary residual dusk-to-dawn 'overshielding' E-field whose duration (barring further rapid IMF changes) is τ_S. A qualitative argument by *Fejer et al.* [1990] suggests that a steady tailward motion of the plasmasheet (i.e., poleward motion of the auroral boundary) during quieting could produce an eastward 'overshielding' E-field, induced by gradual dipolarization of formerly tail-like magnetic field lines, even if the quieting occurs more slowly than τ_S. In this scenario, overshielding could outlast τ_S, with lifetime comparable to the entire magnetic reconfiguration.

Because the overshielding electric field is concentrated in the pre-dawn sector [*Senior and Blanc*, 1984; *Fejer and Scherliess*, 1995] it is there that antisunward motion of cold plasma is most pronounced, creating a shoulder (i.e., a bulge 2–3 MLT hours in extent). Extrapolation of the 29 July shoulder's observed motion back in time [*Burch et al.*, 2001a; *Goldstein et al.*, 2002] puts the shoulder in the pre-dawn sector at ∼17 UT on 28 July, when the IMF turned northward. We propose that overshielding created the 29 July shoulder. As in *Goldstein et al.* [2002], we present calculations of the Magnetospheric Specification Model (MSM) [*Freeman et al.*, 1993; *Wolf et al.*, 1997; *Weiss et al.*, 1997; *Lambour et al.*, 1997]. It will be shown that the MSM-estimated overshielding field is consistent with low-latitude ionospheric drifts seen by ROCSAT-1 on 28 July.

Description of the MSM Model

The MSM computes $E \times B$ drift motion of cold plasma, and is augmented by a simple plasmaspheric refilling algorithm [*Lambour et al.*, 1997]. As initial conditions (ICs) to the model, the plasmapause boundary is specified, and the electron density interior to the plasmapause is assumed to follow the *Carpenter and Anderson* [1992] model. The MSM includes a spatially nonuniform, time-varying parametric E-field model; its functional form is based on characteristic results from the Rice Convection Model (RCM) [*Spiro et al.*, 1988]. The MSM is not self-consistent; it models geomagnetic phenomena by parameterizing the effects of several input quantities: Kp; Dst; solar wind (SW) and interplanetary magnetic field (IMF); ABI (auroral boundary index [*Gussenhoven et al.*, 1983]); and PCP (cross-polar cap potential), inferred for 28-29 July 2000 using *Boyle et al.* [1997]. IMF and SW data were measured by the MAG [*Smith et al.*, 1998] and SWEPAM [*McComas et al.*, 1998] instruments on the ACE spacecraft. At about 16:20 UT on 28 July, ACE MAG recorded a distinctive northward IMF turning at its upstream location $X \approx 250\,R_E$. Using the SWEPAM-measured solar wind speed $V_{SW} \approx 455$ km/s the propagation delay $\Delta t_P \equiv X/V_{SW}$ between ACE and a nominal magnetopause ($10\,R_E$) was 58 ± 5 minutes, where the 5-minute uncertainty was obtained by identifying the 16:20 ACE northward IMF turning in Wind and Geotail data, and using the relative timing of the 3 spacecraft.

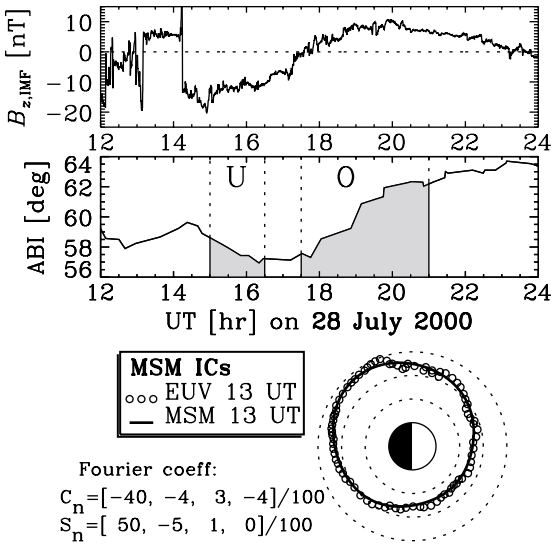

Figure 2. Top: IMF data (ACE MAG), 28 July 2000, the day preceding the shoulder observation in Fig 1. Middle: Auroral boundary index (ABI) [*Gussenhoven et al.*, 1983]. Bottom: 28–29 July MSM run: Initial plasmapause, a Fourier series fit to the 13 UT EUV plasmapause.

MSM Simulation of 28–29 July 2000

Fig 2 shows two input quantities, and ICs for the MSM simulation of 28–29 July 2000. The top panel of Fig 2 shows the propagation-delayed ACE IMF data between 12–24 UT on 28 July. A northward IMF turning at 17:16 UT came after about 3 hours of strong southward IMF ($B_{z,IMF} < 0$). IMF polarity transitions fundamentally effect geomagnetic activity, and this can be reflected in the auroral oval location; e.g., inward plasmasheet motion corresponds to equatorward motion of the aurora. The middle panel shows the ABI index, which represents the equatorward edge of the auroral oval [*Gussenhoven et al.*, 1983]. ABI is inferred from one or more DMSP satellite passes over both north and south poles. To mitigate jitter due to imperfect north/south conjugacy, ABI has been smoothed with a 3-point boxcar average. The MSM's low-latitude E-field algorithm assumes the auroral boundary is near the shielding layer, and they move the same amount. E.g., the model assumes poleward plasmasheet motion is manifested as poleward motion of ABI, and this motion is ascribed to $E \times B$ drift in an eastward E-field. To model this effect the MSM E-field strength is proportional to the time derivative of ABI. Thus, intervals of changing ABI will produce MSM penetration E-fields: dABI/dt < 0 yields undershielding and dABI/dt > 0 yields overshielding. $B_{z,IMF}$ and ABI are correlated; when the IMF changes polarity, dABI/dt changes sign. The bottom panel of Fig 2 shows the initial plasmapause configuration used to start the MSM simulation. The hollow circles trace the plasmapause extracted from the 13 UT EUV image (not shown), mapped to the magnetic equator as in Fig 1. This EUV plasmapause was modeled by a Fourier series: $L_{pp} = 6 + \sum_{n=1}^{4}[S_n \sin(n\varphi) + C_n \cos(n\varphi)]$, where C_n and S_n are listed at the bottom of Fig 2.

The MSM run encompassed 24 hours between 13 UT on 28 July and 13 UT on 29 July. Shaded areas in the middle panel of Fig 2 show intervals of penetration E-field in the MSM. From 15–16:30 UT, the inner magnetosphere was undershielded ('U'), and from 17:30–21:00 UT it was overshielded ('O'). Unshaded areas are when the inner magnetosphere was well-shielded (no significant penetration E-field). The overshielding ('O') interval is considerably longer than the expected value of τ_S [*Kelley et al.*, 1979]; we suggest that this extended period of overshielding arises due to the magnetic reconfiguration effect mentioned earlier.

Fig 3 shows a snapshot of MSM output at 19 UT on 28 July. The Earth is drawn to scale with noon to the right; the white annulus surrounding the Earth is the inner

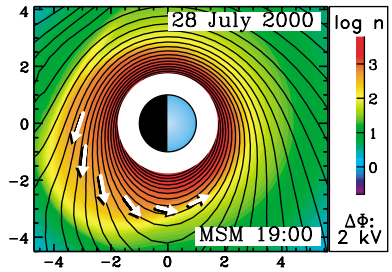

Figure 3. MSM, 19 UT on 28 July 2000: Overshielding causes pre-dawn radial flows, creating the shoulder.

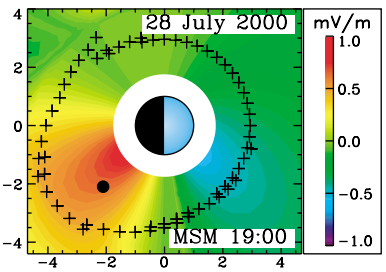

Figure 4. Eastward component E_φ of the penetration E-field during overshielding at 19 UT on 28 July.

boundary of the simulation at 1.8 R_E. Colors are $\log_{10}$ equatorial electron density (cm^{-3}); the plasmapause (defined as a density gradient of magnitude $\geq 100\,cm^{-3}/R_E$ occurring in density range 100–150 cm^{-3}) is yellow-orange. The total electric potential (convection plus corotation) is overlayed on the density colors as black contour lines spaced 2 kV apart. The pre-dawn arrows are flow vectors at $L = 3$, with lengths scaled as 1 R_E = 0.72 R_E/hour. The 19 UT snapshot is taken during an MSM overshielding interval, and captures the formation of the shoulder. The overshielding E-field is strongest in the pre-dawn sector (0–6 MLT), where it points eastward and pushes the plasma radially outward (i.e., antisunward on the nightside). Added to the corotation E-field, this produces the characteristic shape of the shoulder. As found by *Goldstein et al.* [2002] for the 24 May 2000 shoulder, the MLT profile of the magnitude of the radial flow follows the observed shoulder shape in Fig 1. In the MSM simulation, this sort of flow pattern persisted for 3.5 hours, from 17:30–21:00 UT (28 July), moving pre-dawn plasma outward and forming a pre-dawn bulge, evident in Fig 3.

Fig 4 plots the eastward component E_φ of the MSM overshielding field at 19 UT. Colors give intensity of E_φ in mV/m. The crosses follow the local-time shape of the plasmapause of Fig 3. Plasmaspheric E_φ is concentrated in the pre-dawn sector, with peak E_φ value ($\sim$1 mV/m) comparable to outer plasmaspheric corotation-E strength. The pre-dawn E_φ concentration in MSM's overshielding field was established from radar observations [*Fejer and Scherliess*, 1995] and is in accord with theoretical calculations of *Senior and Blanc* [1984] and *Spiro et al.* [1988]. Fig 4 also shows a lesser concentration of westward E-field in the pre-noon sector, centered at about 9 MLT. This westward E-field weakly pushes plasma radially inward at MLT values east of the shoulder, accentuating its shape and creating a radial-flow reversal near the dawn terminator. Later we show this pre-dawn flow concentration and dawn flow reversal are found in ROCSAT-1 ion drift data.

E_φ was sampled at $L = 3$, at MLT values corresponding to a corotating flux tube: MLT = 3 + (UT − 19). At 19 UT this flux tube is at $[L, \mathrm{MLT}] = [3, 3]$, as indicated by the filled circle in Fig 4. The sampled E_φ and corresponding radial flows V_r are plotted versus UT in Fig 5. Overshielding occurs when dABI/dt > 0, so E_φ peaks occur at the strongest jumps in ABI. These peaks, and some of the rapid time variation of E_φ and V_r, may be unphysical results of ABI jitter (mentioned above) and discrete ABI time-sampling. When ABI starts to level off after 20 UT, the overshielding E-field subsides. The mean overshielding E_φ (0.5 mV/m) and mean associated flow speed (0.3 R_E/hour) should not be extremely sensitive to the ABI sampling irregularities discussed above. Multiplied by 3.5 hours of overshielding, this yields radial shoulder size of 1 R_E, roughly consistent with the shoulder size seen by EUV. The 29 July shoulder's radial size was 2–3 times that of 24 May 2000. In the 24 May event, 2 sudden strong northward IMF transitions occurred in succession, producing 45 accumulated minutes of MSM peak flow speeds of 0.72 R_E/hr [*Goldstein et al.*, 2002]. In the 29 July event, the IMF turned gradually from strong southward to strong northward, producing 3.5 hours of 0.3 R_E/hr overshielding flows, i.e., half as strong as that of 24 May but lasting 5 times as long. This easily accounts for the size difference, and also implies that overshielding can indeed arise from an extended quieting period.

Although the MSM probably captures the mechanism of shoulder formation in this case, the location and shape of the MSM shoulder do not agree perfectly with observations. Fig 6 compares the MSM simulated plasmapause at 3:00 UT with the 2:57 EUV plasmapause of Fig 1. The 2:57 EUV shoulder is plotted as filled circles. The 3:00 MSM shoulder (dotted line) is offset in both L and MLT relative to EUV. The solid line is the MSM shoulder, shifted by 1.6 MLT-hours and $-0.6\,R_E$ to agree with the EUV shoulder location. The radial offset may be due to brief periods of unrealistically large E_φ due to the ABI 'jitter' mentioned above. The MLT offset may be attributable to the idealized nature of MSM's E-field. The azimuthal dependence of the MSM penetration E-field was developed by comparing RCM results to statistical analysis of Jicamarca radar data, and thus cannot capture all the small-scale variations in the actual penetration E-field of a particular day. In addition to the location offset, the shape of the MSM shoulder is noticably less distinct than in the EUV data. This blurring is attributed to numerical diffusion in the MSM code. Taking into consideration the MSM's numerical diffusion and imperfect E-field model that can both contribute to time-accumulated errors and innaccurate flow fields, and the ABI jitter that creates unphysical effects in the model E-field, the MSM-EUV

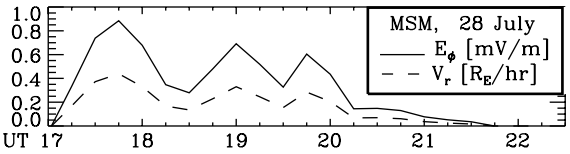

Figure 5. Eastward electric field E_φ and radial flow speed V_r versus UT for a corotating $L = 3$ flux tube.

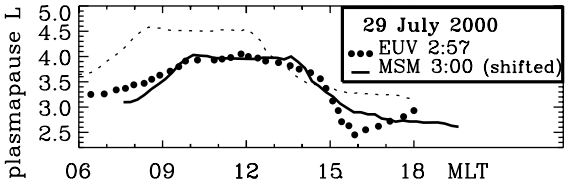

Figure 6. 29 July shoulder L-value vs. MLT, as seen by EUV (filled circles); MSM (dotted line); MSM, shifted by $[-0.6\,R_E, 1.6\ \mathrm{MLT}]$ (solid line).

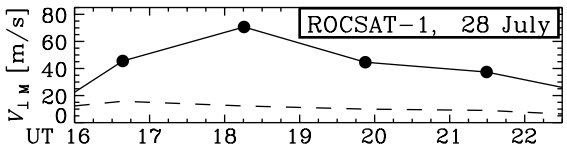

Figure 7. ROCSAT-1 data, 28 July, during shoulder formation. $V_{\perp M}$ (solid line) maps to pre-dawn (0–6 MLT) radial flow in equatorial plane. Six-day average flow from 25-27 and 29-31 July (dashed line) has been subtracted off.

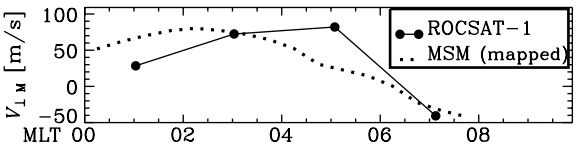

Figure 8. MLT-profile of radial flows: ROCSAT-1 during 17:30–19 UT (solid line) and MSM at 17:45 (dotted). MSM flows have been mapped to $L \approx 1.1$. Outward pre-dawn flow and dawn flow reversal evident in both.

agreement is reasonably good. Based on MSM-EUV comparisons alone, overshielding was very likely responsible for the 29 July shoulder, and the spatial form and time-averaged strength of the MSM overshielding field are both reasonable.

ROCSAT-1 Observation of Shoulder Formation

ROCSAT-1 follows a 1.6-hour circular orbit with 35 degree inclination, at 600 km altitude, sampling the low-latitude ionosphere. Fig 7 shows ion drift meter data from 16–22 UT on 28 July. Plotted are values of $V_{\perp M}$, the velocity component perpendicular to the geomagnetic field in the meridional plane. Each data point (filled circle) is an average of $V_{\perp M}$ measurements taken in the 0–6 MLT (pre-dawn) range during a single orbit, plotted versus the UT when ROCSAT-1 crossed 0 MLT. $V_{\perp M}$ corresponds in the equatorial plane to radial flows at $L \approx 1.1$. Enhanced $V_{\perp M}$ during 17–21 UT is certainly consistent with the MSM-predicted eastward overshielding field in the pre-dawn sector. However, interpretation of low-latitude ionospheric fields is complicated by effects of neutral winds that usually dominate. To address this, the dashed line in Fig 7 plots pre-dawn $< V_{\perp M} >$, averaged over the 6 quieter surrounding days 25–27 July and 29–31 July. The plotted $V_{\perp M}$ data, which have had this 6-day average $< V_{\perp M} >$ subtracted off, are clearly well above the 6-day average. The peak near 18 UT on 28 July was the highest measured flow in the 7-day period 25–31 July. Thus for this event the prompt-penetration E-field apparently dominated over neutral wind effects. The UT profile of orbit-averaged pre-dawn $V_{\perp M}$ is in rough qualitative agreement with that predicted by MSM (Fig 5).

The MLT profile of the ROCSAT-observed flows is also consistent with MSM predictions. Fig 8 shows $V_{\perp M}$ (filled circles), averaged over the UT interval 17:30–19:00 with each point including 2 hours MLT, plotted versus MLT. For comparison, a 17:45 UT MSM curve V_r (dotted line) is shown. The MSM's inner boundary is at $L = 1.8$ (well above the ROCSAT-1 $L \approx 1.1$), so the MSM V_r was extrapolated to $L = 1.1$ assuming $V_r \propto L^3$. The ROCSAT-1 and MSM curves both show quantitatively comparable outward pre-dawn plasma motion, with a flow reversal near the dawn terminator (post-dawn plasma moves inward) as seen in Figs 3 and 4. The MSM peak is about 1.6 MLT-hours west of the ROCSAT-1 peak, and the MSM dawn flow reversal is not nearly as sharp as that of ROCSAT-1; both these differences are consistent with the differences between the MSM and EUV shoulders at ~ 3 UT (Fig 6) discussed earlier.

3. Conclusion

We have shown that the shoulder observed by IMAGE EUV on 29 July 2000 was probably created the previous day by overshielding during 17–21 UT. This event is notable in that overshielding apparently resulted from a gradual, rather than a sudden change in IMF polarity. MSM simulation estimates for the overshielding field are consistent with ROCSAT-1 ion drift measurements. The ROCSAT-1 data indicate (a) outward radial flow of magnitude comparable to that predicted by MSM in the pre-dawn sector and (b) an MLT profile of the overshielding flows that contains a pre-dawn peak and a dawn flow-reversal, consistent with both MSM and the observed shoulder shape. ROCSAT-1 data suggest that the prompt-penetration field was unusually large, dominating low-latitude ionospheric neutral wind effects; this strong penetration-E is consistent with the large radial size of the shoulder.

Acknowledgments. We thank N. Ness, C. Smith and the ACE science center (ACE MAG); D. McComas (ACE SWEPAM); F. Rich (ABI); Kyoto WDC-C2 web site (Dst); and NGDC (Kp). Wind/Geotail data browsed on CDAWeb. NASA contract NAS5-96020 with SwRI supported work at Rice and U. Arizona. Some work at Rice supported by NASA SEC Theory program, under ATM NAG5-11881. ROCSAT supported by NSC90-2111-M-008-045-AP3 from National Science Council of the Republic of China.

References

Boyle, C. B., P. H. Reiff, and M. R. Hairston, Empirical polar cap potentials, *J. Geophys. Res.*, *102*, 111, 1997.

Burch, J. L., D. G. Mitchell, B. R. Sandel, P. C. Brandt, and M. Wüest, Global dynamics of the plasmasphere and ring current during magnetic storms, *Geophys. Res. Lett.*, *28*, 1159, 2001a.

Burch, J. L., et al., Views of Earth's magnetosphere with the IMAGE satellite, *Science*, *291*, 619, 2001b.

Carpenter, D. L., and R. R. Anderson, An ISEE/Whistler model of equatorial electron density in the magnetosphere, *J. Geophys. Res.*, *97*, 1097, 1992.

Fejer, B. G., and L. Scherliess, Time dependent response of equatorial ionospheric electric fields in magnetospheric disturbances, *Geophys. Res. Lett.*, *22*, 851, 1995.

Fejer, B. G., R. W. Spiro, R. A. Wolf, and J. C. Foster, Latitudinal variation of perturbation electric fields during magnetically disturbed periods: 1986 SUNDIAL observations and model results, *Ann. Geophys.*, *8*, 441, 1990.

Freeman, J. W., R. A. Wolf, R. W. Spiro, G.-H. Voigt, B. A. Hausman, B. A. Bales, R. V. Hilmer, A. Nagai, and R. L. Lambour, Magnetospheric Specification Model development code and documentation. Report for USAF contract F19628-90-K-0012, Rice University, Houston, TX, 1993.

Goldstein, J., R. W. Spiro, P. H. Reiff, R. A. Wolf, B. R. Sandel, J. W. Freeman, and R. L. Lambour, IMF-driven overshielding electric field and the origin of the plasmaspheric shoulder of May 24, 2000, *Geophys. Res. Lett.*, *29*, 10.1029/2001GL014534, 2002.

Gussenhoven, M. S., D. A. Hardy, and N. Heinemann, Systematics of the equatorward diffuse auroral boundary, *J. Geophys. Res.*, *88*, 5692, 1983.

Kelley, M. C., B. G. Fejer, and C. A. Gonzales, An explanation for anomalous ionospheric electric fields associated with a northward turning of the interplanetary magnetic field, *Geophys. Res. Lett.*, *6*, 301, 1979.

Lambour, R. L., L. A. Weiss, R. C. Elphic, and M. F. Thomsen, Global modeling of the plasmasphere following storm sudden commencements, *J. Geophys. Res.*, *102*, 24351, 1997.

McComas, D. J., S. J. Bame, P. Barker, W. C. Feldman, J. L. Phillips, P. Riley, and J. W. Griffee, Solar wind electron proton alpha monitor (SWEPAM) for the Advanced Composition Explorer, *Space Sci. Rev.*, *86*, 563, 1998.

Senior, C., and M. Blanc, On the control of magnetospheric convection by the spatial distribution of ionospheric conductivities, *J. Geophys. Res.*, *89*, 261, 1984.

Smith, C. W., M. H. Acuna, L. F. Burlaga, J. L'Heureux, N. F. Ness, and J. Sheifele, The ACE magnetic field experiment, *Space Sci. Rev.*, *86*, 613, 1998.

Spiro, R. W., R. A. Wolf, and B. G. Fejer, Penetration of high-latitude-electric-field effects to low latitudes during SUNDIAL 1984, *Ann. Geophys.*, *6*, 39, 1988.

Weiss, L. A., R. L. Lambour, R. C. Elphic, and M. F. Thomsen, Study of plasmaspheric evolution using geosynchronous observations and global modeling, *Geophys. Res. Lett.*, *24*, 599, 1997.

Wolf, R. A., J. W. Freeman Jr., B. A. Hausman, R. W. Spiro, R. V. Hilmer, and R. L. Lambour, Modeling convection effects in magnetic storms, in *Magnetic Storms,* Geophysical Monograph 98, edited by B. T. Tsurutani, p. 161, American Geophysical Union, Washington, D. C., 1997.

J. Goldstein, R. W. Spiro, R. A. Wolf, P. H. Reiff, Dept of Physics & Astronomy, Rice University, Houston, TX 77005 USA (jerru@rice.edu) B. R. Sandel, Lunar and Planetary Lab, University of Arizona, Tucson, AZ 85721 USA S.-Y. Su, Institute of Space Science, National Central University Taiwan, ROC

(Received _____.)